XV-15 Rotor Simulation in Flow360 using the Blade Element Theory

John Moore
Principal Research Engineer
FlexCompute, Inc
Belmont, MA, USA

Feilin Jia
Research Scientist
CFD Technology Lead
FlexCompute, Inc
Belmont, MA, USA

Qiqi Wang
Co-founder
FlexCompute, Inc
Belmont, MA, USA
Associate Professor
Massachusetts Institute of Technology
Cambridge, MA, USA

ABSTRACT

This paper presents results of the numerical study of the Bell XV-15 rotor with the flow solver Flow360 using a coupled Navier-Stokes/Blade Element Theory model. Results are presented for both steady-state and transient simulations. The resulting thrust, torque, and blade loadings show good agreement with high-fidelity DDES results computed with Flow360 and experiments.

NOTATION

R	=	rotor disk radius
N_b	=	number of blades
A	=	rotor disk area, πR^2
c	=	blade chord
c_{bl}	=	blade line chord
σ	=	local solidity
t	=	thickness of BET disk
c_{ref}	=	reference blade chord
C_Q	=	rotor torque coefficient, $Q/(\rho\Omega^2R^3A)$
C_T	=	rotor thrust coefficient, $T/(\rho\Omega^2R^2A)$
FoM	=	figure of merit, $\frac{C_T^{3/2}}{\sqrt{2}C_Q}$
η	=	propulsive efficiency, $\eta = C_T V_{\text{inf}}/(C_Q V_{tip})$
T	=	rotor thrust
Q	=	rotor torque
Ω	=	rotor angular speed
$\hat{a}$	=	disk unit axial direction
$\hat{c}$	=	disk unit circumferential direction
$\mathbf{v_f}$	=	local fluid velocity
Φ	=	local disk flow angle
α	=	local angle of attack
β	=	local blade twist angle
M_{tip}	=	tip Mach number
Re	=	Reynolds number
θ_{75}	=	blade pitch at 75 percent radius
μ	=	advance ratio
c_{ref}	=	reference chord

Presented at the Vertical Flight Society's 78th Annual Forum & Technology Display, Ft. Worth, Texas, USA, May 10–12, 2022.

INTRODUCTION

Unlike typical helicopter rotors, tiltrotor blades demand a compromised design to operate efficiently in both helicopter and propeller modes. Because of its complexity in geometry and widely varying operation conditions, many experimental investigations of the rotor performance of the XV-15 tiltrotor have been done over the years. In 1971, the first substantial experimental wind tunnel study of the XV-15 was performed by Anon (Ref. 1) at Nasa Ames. In 1985, a comprehensive experimental study of the XV-15 tiltrotor in helicopter mode was conducted by Felker et al. (Ref. 2) at the NASA-Ames Outdoor Aeronautical Research Facility (OARF). In 1997, Light (Ref. 3) conducted hover and forward flight tests in the 80-fit by 120-ft Wind Tunnel, but the number of tested operation conditions are relatively limited. To fill the gap, in 2002, Betzina did a series of experiments on hovering flight and propulsive/descending forward flight in helicopter mode, and then an extensive data set was published (Ref. 4).

In recent decades, both computer hardware and numerical algorithms have evolved and advanced dramatically, which makes computational fluid dynamics (CFD) a powerful tool to predict rotor performance. Significant efforts have been performed to develop various numerical methods to improve the accuracy of CFD simulations on tiltrotors compared with the published experimental data. The simplest method was analytical models based on the actuator disk theory and the blade element momentum theory (Ref. 5), but it ignores the blade-vortex interaction and the effect of rotor wake. Due to the emergence of parallel computers, modern high fidelity approaches based on full-domain numerical simulation of the Navier-Stokes equations were gradually employed. Kaul et al. (Ref. 6) and Yoon et al. (Ref. 7) conducted simulations

on the hovering XV-15 main rotor blade using OVERFLOW CFD code. Gates (Ref. 8) and Garcia et al (Ref. 9) used Helicopter Multi-Block (HMB) CFD solver to perform detailed performance analyses of the hover and propeller modes of the XV-15 blades.

In the past decade, hybrid CFD-Blade Element Theory (BET) methods have been developed in order to reduce the cost of performing rotor simulations while retaining a high level of fidelity. Both steady-state (Refs. 10–12) and transient (Ref. 13) models have been developed. This paper presents results for a coupled BET-RANS solver implemented withing Flow360. Both steady-state (denoted BET-Disk) and transient (denoted BET-Line) models are presented.

BLADE ELEMENT THEORY

The RANS equations are coupled with the Blade Element Theory through a source term applied to the Navier-Stokes equations. The fictitious blades produce a force on the flow field according to the velocity the local airfoil section observes. Each blade section is treated as a two-dimensional airfoil. The blade rotational speed, twist distribution, chord distribution, and sectional airfoil polars are used to compute the c_d and c_l at every location along the blade based on the local flow velocity. These lift and drag coefficients prescribe a forcing term to the momentum components of the Navier-Stokes equation. The flowfield then evolves, and an updated velocity field is fed back into the BET model and this process continues until nonlinear convergence is reached.

The blade-relative velocity and the circumferential and axial components of this velocity can be computed according to equation 1.

$$\begin{aligned} \mathbf{v_{rel}} &= \mathbf{v_f} - \Omega r\hat{c} \\ v_{cir} &= \mathbf{v_{rel}} \cdot \hat{c} \\ v_{ax} &= \mathbf{v_{rel}} \cdot \hat{a} \end{aligned} \tag{1}$$

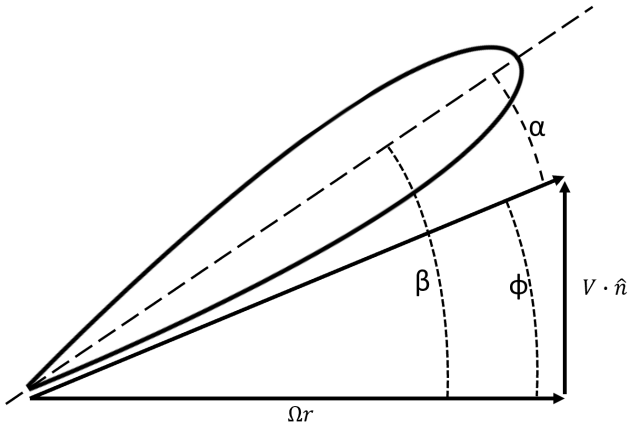

Figure 1. BET nomenclature for an blade airfoil section

The local disk flow angle ϕ can then be computed as

$$\phi = atan2(v_{ax}, v_{cir}) \tag{2}$$

and the angle of attack is evaluated as according to Figure 1

$$\alpha = \beta - \phi \tag{3}$$

The lift and drag coefficients, c_l and c_d are obtained through linear interpolation of airfoil polar lookup tables. Currently, Flow360 performs a four-dimensional interpolation across Mach number, Reynolds number, radial location r, and α to obtain the sectional coefficients. Once the sectional lift and drag coefficients are evaluated, the axial and circumferential sectional coefficients are computed as:

$$\begin{aligned} c_{f_a} &= c_l cos(\phi) + c_d sin(\phi) \\ c_{f_c} &= -c_d cos(\phi) + c_l sin(\phi) \end{aligned} \tag{4}$$

It has been determined that the standard tip loss factor used in the Blade-Element momentum theory is not needed for BET-CFD applications, because the CFD solver will model the vortex tip roll-up. Therefore, the results presented in this work do not include a tip loss factor.

The axial and circumferential forces at each node within the BET disk can now be evaluated as

$$\begin{aligned} F_{ax} &= \frac{1}{2t}\rho \|\mathbf{v_{rel}}^2\| \sigma W_t c_{f_a} \\ F_{cir} &= \frac{1}{2t}\rho \|\mathbf{v_{rel}}^2\| \sigma W_t c_{f_c} \end{aligned} \tag{5}$$

F_{ax} and F_{cir} are applied to the momentum components of the Navier-Stokes equations as forcing terms. The local solidity σ depends on the type of analysis run. For the BET-Disk formulation, local solidity is defined as:

$$\sigma = \frac{N_b c}{2\pi r} \tag{6}$$

whereas for the BET-Line formulation the local solidity is defined as:

$$\sigma = \frac{c}{c_{bl}} \lambda W_c \tag{7}$$

where W_t and W_c are weighting functions of the distance to the disk or blade, defined as:

$$\begin{aligned} W_t(x) &= 2cos^2(\pi x/t) \\ W_c(x) &= 2cos^2(\pi x/c_{bl}) \end{aligned} \tag{8}$$

λ is a tuning parameter introduced into the BET-Line model in order to counter changes in the local velocity field due to the line vortex. Numerical experiments have shown $\lambda = 4/\pi$ to be a reasonable value for this parameter when $c_{bl} \approx t$, although further investigation into the effect of this parameter on other geometries and flight conditions would be beneficial.

XV-15 GEOMETRY, MESHES, AND POLARS

The CFD model of XV-15 rotor was generated based on the experiment by Felker (Ref. 2).

Table 1. XV-15 Rotor airfoil specification.

r/R	Airfoil
0.09	NACA 64-935
0.17	NACA 64-528
0.51	NACA 64-118
0.80	NACA 64-(1.5)12
1.00	NACA 64-208

Geometry

The rotor blade consists of 5 NACA 6-series aerofoil sections, which are reported in Table 1.

The radius of the three-bladed rotor is 150 inches. The inboard aerodynamic section starts at 9.1% radius with a chord of 16.6 inches, linearly tapering a chord of 14 inches by 25% radius. The chord keeps a constant 14 inches from 25% radius to the tip. Each blade has a structural twist angle of -40.25° from the root cutoff to the tip. The main geometric characteristics of the XV-15 rotor blades are listed in Table 2. Also, a detailed sketch of the XV-15 blade radial twist and chord distributions are shown in Figure 2.

Table 2. Geometric properties of the full-scale XV-15 rotor

Parameter	Value
Number of blades, N_b	3
Rotor radius, R	150 inches
Reference blade chord, c_{ref}	14 inches
Aspect ratio, R/c_{ref}	10.71
Rotor solidify, σ	0.089
Linear twist angle, Θ	-40.25°

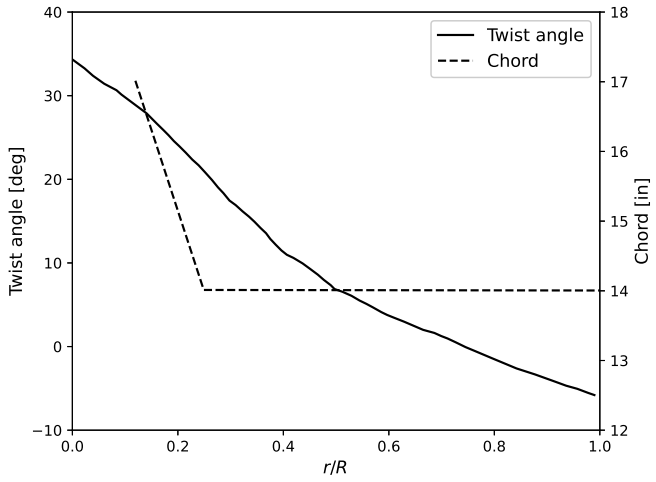

Figure 2. XV-15 rotor blade's twist and chord radial distribution (Ref. 2).

Meshes

Pointwise® was used to create two meshes which were used to generate the results presented in this paper, one for the propeller and hovering condition, and another for the helicopter condition. A mesh refinement study was performed using the BET-Disk solver and the 10° pitch hovering condition to determine the required mesh resolution. A series of meshes was generated, ranging from 188K to 2.3M nodes. The meshes consist of a single block, with the far-field located 50 disk radiuses from the center of the domain. Figure 3 shows that the

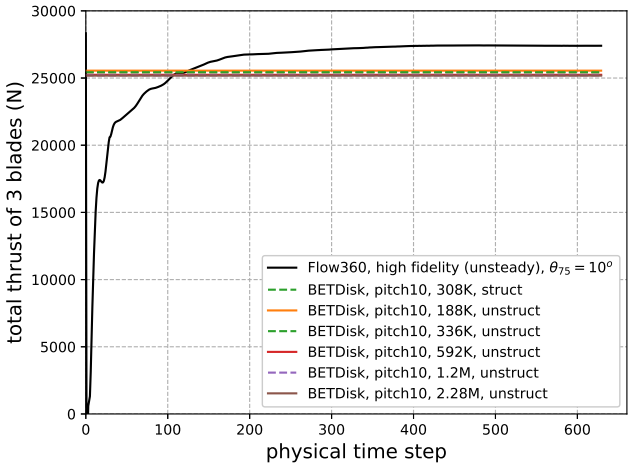

Figure 3. Mesh convergence for hovering condition, $\theta_{75} = 10^\circ$

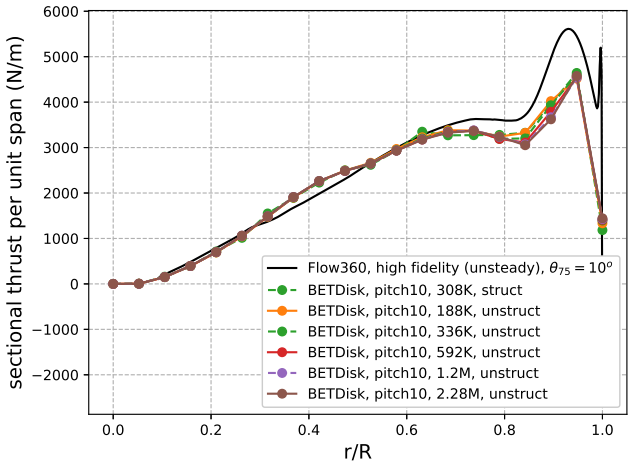

Figure 4. Mesh convergence of sectional thrust loading in hovering condition, $\theta_{75} = 10^\circ$

thrust is relatively insensitive to the mesh coarseness. There is a 0.6% difference in the converged thrust between the finest and coarsest mesh. We have, however, noticed more significant sensitivity to the thickness, t, of the disk region. Figure 4 demonstrates the convergence of the sectional thrust loading as the mesh size is increased. The 592K node grid shows little difference in loading compared to the finer loading. Nonetheless, we ran all cases in this work using the finest grid since each case only requires several minutes of runtime.

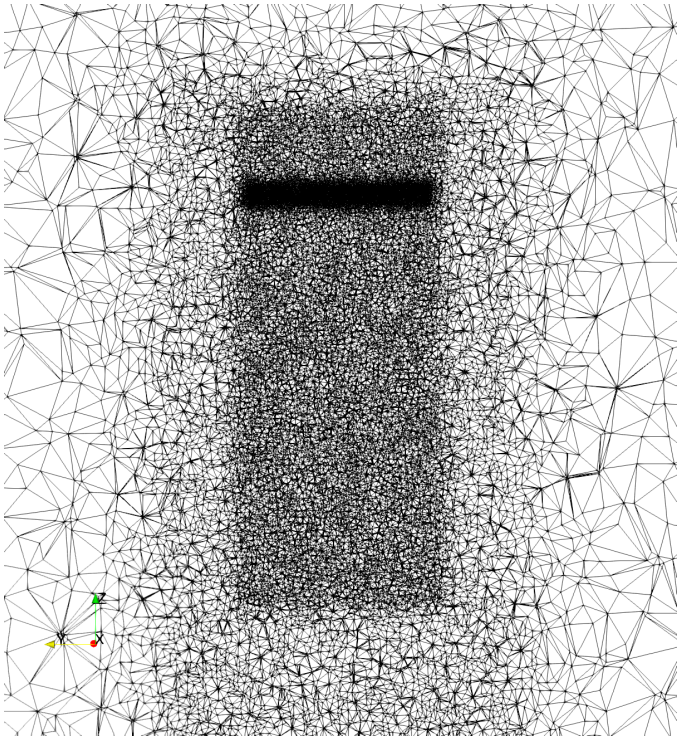

Figure 5. 592K node disk-resolving mesh, similar refinement to the 2.3M node mesh for the hovering and airplane condition simulations.

The helicopter configuration involves more complex physics; therefore we generated a larger mesh consisting of 4.1M nodes to better resolve the wake and the blade/tip vortex interactions. The mesh in the immediate region of the blade disks and lines was meshed to an edge size of $0.01R$ for both meshes. In this work we chose $c_{bl} = t = 15$ inches for both meshes. Choosing c_{bl} and t to be on the order of the reference chord length has yielded good results so far, although further work is necessary to minimize the sensitivity of the BET models to these parameters.

Airfoil Polars

The lift and drag polars for the airfoil cross sections were predicted using XFOIL (Ref. 14). The polars were computed under the assumption of a Reynolds number of 5e6 and incompressible flow. XFOIL was not able to converge several airfoils at some of the higher Mach number conditions. Future studies will assess the impact of compressibility-adjusted polars on the results of the BET simulations.

NUMERICAL RESULTS

Experimental results from the XV-15 rotor are available for three flight regimes: hovering, airplane, and helicopter mode. This work compares BET-Disk and BET-Line method results to both high fidelity DDES computed using Flow360, and experimental data for these three operating regimes. The flight conditions evaluated in this work are detailed in table 3.

Table 3. Flow conditions for the full-scale XV-15 tiltrotor blade.

	Hover	Helicopter	Airplane
M_{tip}	0.69	0.69	0.54
Re	4.95e6	5.65e6	4.50e6
θ_{75}	0°,3°,5°,10°,13°	2°-10°	26°,27°,28°,28.8°
α		-5°,0°,5°	-90°
μ		0.170	0.337
nodes	2.3M	4.1M	2.3M

Airplane Mode

The airplane mode configuration is considered first. In this configuration, the blades are tilted forward as in a typical turboprop and the aircraft is flying horizontally. This should be the easiest operating condition to accurately simulate since there is no blade/tip-vortex interaction. We compute the steady-state solution using the BET-Disk method, and use the BET-Line method to compute the transient solution. The BET-Disk simulations typically converge within 600 pseudo steps, using a $CFL_{max} = 200$. The BET-Line simulation is run for 10 revolutions, with a time step corresponding to two degrees per step. The forces were well converged after 10 revolutions. Figures 6 and 7 show C_Q and η as a function of C_T, respectively. The experimental results by Anon (Ref. 1) corresponds to the following series of collective pitch angles: $[23.7°, 24.8°, 25.5°, 27.5°, 28.0°]$

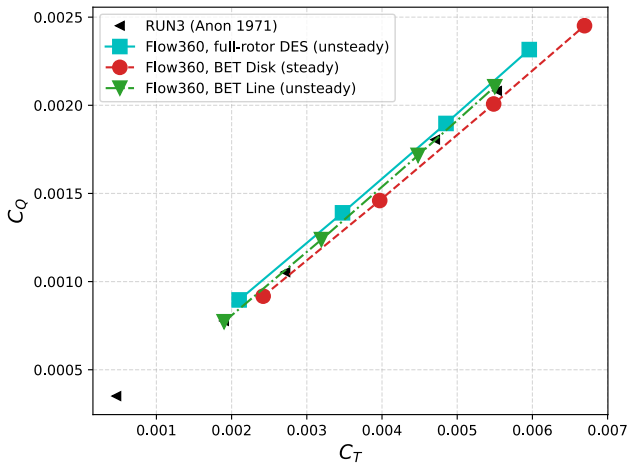

Figure 6. C_T and C_Q comparison between BET-Disk, BET-Line, Flow360 DDES, and experiments for airplane mode, $\theta_{75} = 26°, 27°, 28°, 28.8°$

Figure 6 shows good agreement between both BET-Line and BET-Disk compared to the high-fidelity results. The BET-Disk method slightly over-predicts both thrust and torque compared to the DDES simulation, whereas the BET-Line method under-predicts both thrust and torque.

Both the BET-Line and BET-Disk methods compare well to

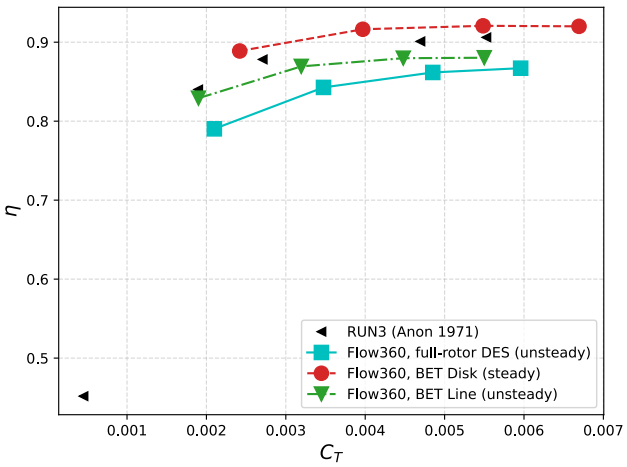

Figure 7. C_T vs η comparison between BET-Disk, BET-Line, Flow360 DDES, and experiments for $\theta_{75} = 26^\circ, 27^\circ, 28^\circ, 28.8^\circ$

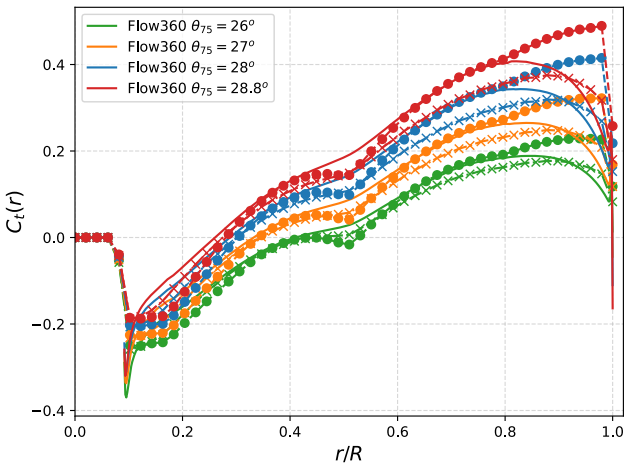

Figure 8. Sectional thrust coefficient in airplane mode compared to full-rotor Flow360 DDES. Solid line is DDES, circle markers are BET-Disk, and cross markers are BET-Line

the high fidelity model and experiment in terms of estimating propulsive efficiency, η, defined in the nomenclature. The BET-Disk method over-predicts efficiency compared to both experiment and DDES, while the BET-line method predicts an efficiency between the experiment and DDES.

In addition to comparing the total C_T and C_Q, it is often useful to compare the sectional thrust and torque loadings. These loadings are defined as:

$$C_t(r) = \frac{dF_{ax}/dr}{\frac{1}{2}\rho_\infty(\Omega r)^2 c_{\text{ref}}} \cdot \frac{r}{R} \tag{9}$$

$$C_q(r) = \frac{dF_{cir}/dr}{\frac{1}{2}\rho_\infty(\Omega r)^2 c_{\text{ref}} R} \cdot \frac{r}{R} \tag{10}$$

Figure 8 shows the thrust loading for all pitch conditions simulated in airplane mode. The steady-state BET-disk method over-predicts the thrust loading near the tip, whereas the transient BET-line method tends to under-predict the thrust loading in the mid-blade region compared to DDES. Figure 9 compares the sectional torque loading of BET-Disk, BET-Line, and Flow360 DDES. Much like the thrust loading, the BET-Disk method tends to over-predict the torque loading near the tip, and the BET-Line method under-predicts the torque with respect to the high-fidelity results. This is consistent with the total $C_Q - C_T$ and $\eta - C_T$ plots in figures 6 and 7.

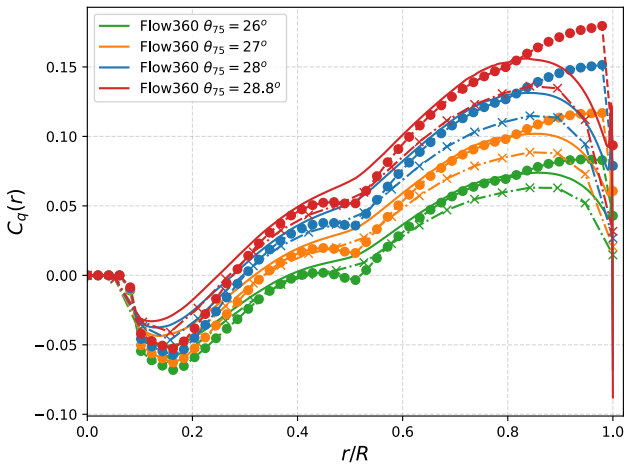

Figure 9. Sectional torque coefficient in airplane mode compared to full-rotor Flow360 DDES. Solid line is DDES, circle markers are BET-Disk, and cross markers are BET-Line

Hovering Mode

The hovering flight condition presents more of a challenge for lower-fidelity methods, since there are often blade-vortex interaction and highly three-dimensional effects. Similar to the propeller mode condition, each case is run for 10 revolutions with a time step corresponding to two degrees per step. C_T and C_Q compared to Flow360 DDES and experimental results are shown in Figure 10.

The BET-Disk and BET-Line method both under-predict thrust and torque compared to DDES; however the under-prediction of torque with BET-Disk method is more pronounced. Figure 11 shows the Figure of Merit as a function of C_T for the hovering condition. The BET-Disk method over-predicts the FoM by as much as 10% due to under-prediction of the torque. The BET-Line method also slightly over-predicts efficiency at lower blade loadings, but is in line with the high-fidelity and experimental efficiency for larger blade loadings. Delving into the sectional thrust and torque loadings may provide a deeper understanding of these results. Figure 12 shows very good agreement in sectional thrust loading between the BET and high-fidelity methods. At higher blade loadings, differences appear near the tip, in the last 20%

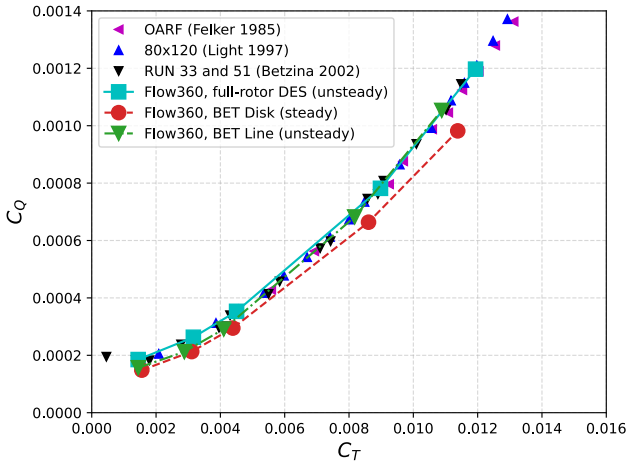

Figure 10. C_T and C_Q comparison between BET-Disk, BET-Line, Flow360 DDES for $\theta_{75} = 0°, 3°, 5°, 10°, 13°$ and experimental results

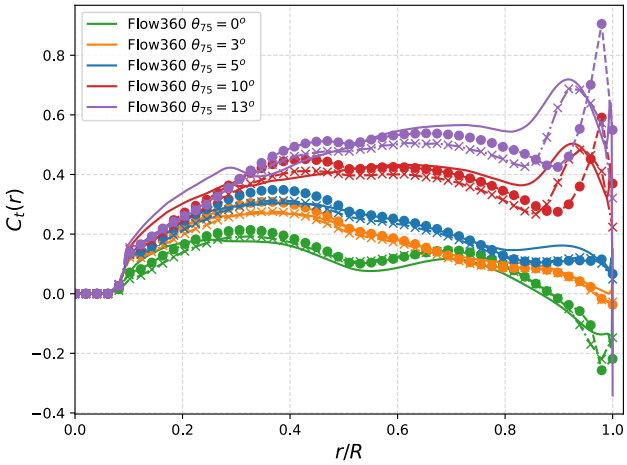

Figure 12. Sectional thrust coefficient compared to full-rotor Flow360 DDES. Solid line is DDES, circle markers are BET-Disk, and cross markers are BET-Line

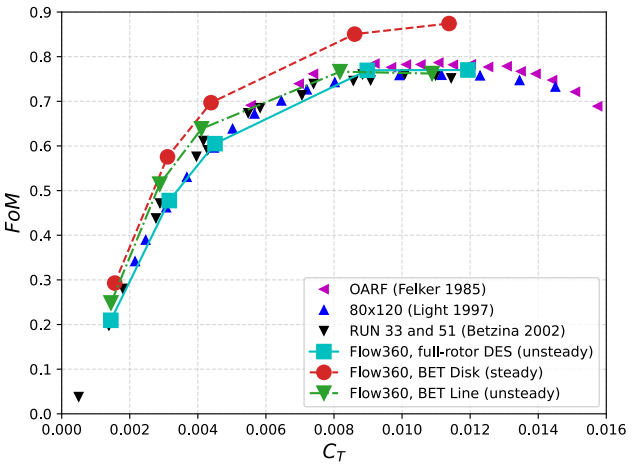

Figure 11. C_T and FoM comparison between BET-Disk, BET-Line, Flow360 DDES for $\theta_{75} = 0°, 3°, 5°, 10°, 13°$ and experimental results

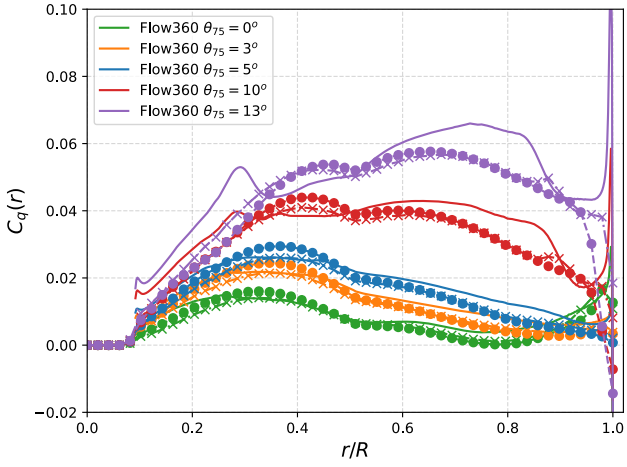

Figure 13. Sectional torque coefficient compared to full-rotor Flow360 DDES. Solid line is DDES, circle markers are BET-Disk, and cross markers are BET-Line

of the blade. Notably, the BET-Disk method over-predicts the thrust at the extremity of the blade. The BET-Line method is more in-line with the DDES loading, although it tends to under-predict the thrust coefficient around $85\%R$. This mismatch is caused by the highly three-dimensional nature of the flow in the region, due in part to the interaction of the leading blade's tip vortex strongly interacting with the blade. Figure 13 shows the sectional torque loading for the three methods. Again reasonable agreement is seen between all models for lower blade loadings (pitches). However, for higher loadings both the BET-Disk and BET-Line under-predict torque especially at $r/R > 0.5$ BET-Disk under-predicts torque more significantly very close to the tip than the BET-Line method. A possible reason for the under-prediction of torque in this region is the use of incompressible airfoil polars in the BET lookup tables. It is worth noting that the DDES method always predicts a spike in C_q at the tip, while the BET methods do not capture this effect.

Helicopter Mode

The most challenging condition to simulate is the helicopter-mode due to the complex blade-vortex interactions. This flight condition is characterized by a forward velocity with the axis of rotation nominally perpendicular to the forward velocity, typically with some incidence angle α. A positive alpha results in the freestream flow entering the disk from below, and is typical of a descending condition. A positive alpha results in the freestream entering the disk from above, as is typically the case for level forward flight or ascending flight. As for the previous two conditions, we also run 10 revolutions for the BET-Line simulations with a time step corresponding to two

degrees per step. Results are averaged over the last revolution. We consider a pitch sweep for three conditions, $\alpha = -5^\circ$, $\alpha = 0^\circ$, and $\alpha = 5^\circ$. The pitch varies from 2° to 10°, with the exact range depending on the angle of attack.

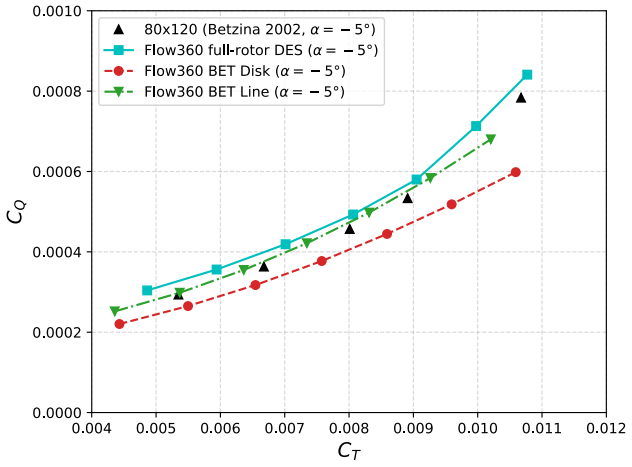

Figure 14. C_T **vs** C_Q **curve for helicopter mode,** $\alpha = -5^\circ$**,** $\theta_{75} = 4^\circ - 10^\circ$

Figure 14 shows C_Q as a function of C_T compared to high fidelity CFD and experimental results for the $\alpha = 5^\circ$ condition and several pitch angles. The BET-Disk method again under-predicts C_T and C_Q compared to experiments and DDES, although C_Q to a greater extent. The BET-Line method predicts slightly less thrust than the BET-Disk method, but the torque is closer to high-fidelity results, especially for smaller pitch angles. Figures 15 and 16 show the C_T-C_Q plot for

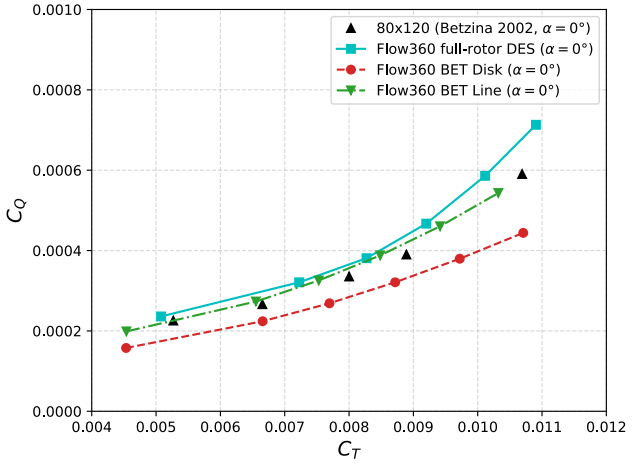

Figure 15. C_T **vs** C_Q **curve for helicopter mode,** $\alpha = 0^\circ$**,** $\theta_{75} = 3^\circ - 9^\circ$

$\alpha = 0^\circ$ and $\alpha = 5^\circ$, respectively. The trend is similar to the -5° case, with BET-Disk under-predicting torque especially at larger pitch angles. The BET-Line method performs better, and the trend line is similar to that of the high fidelity and experimental results.

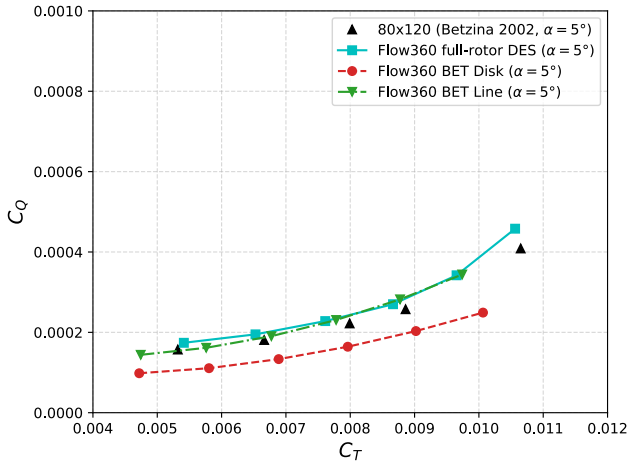

Figure 16. C_T **vs** C_Q **curve for helicopter mode,** $\alpha = 5^\circ$**,** $\theta_{75} = 2^\circ - 7^\circ$

The blade thrust and torque loading distributions were compared to assess differences between the BET model and the high-fidelity results. Figures 17 and 18 show the distribution of C_t and C_q along blade 1 at $\psi = \Omega t = 300^\circ$. It can be observed that there is a discrepancy along the inboard section of the blade. More detailed observation of the DDES results has revealed that this area of the blade is subject to large degrees of radial flow, which may not be accurately modeled by the BET method.

Figure 19 shows the Q-criterion computed for the helicopter mode condition for both BET-Line and Flow360 DDES. The shed vortices interact with the other blades and convect downstream very similarly between the two methods. There are differences in the vortex structures near the blade root; however this region of the rotor only has a small effect on overall rotor performance due to it's low rotational velocity.

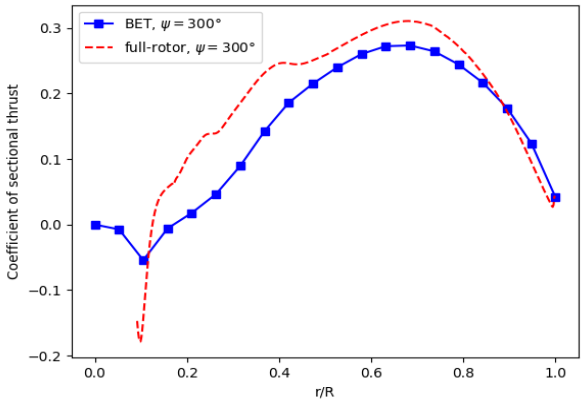

Figure 17. Sectional C_t **on blade 1 at** $\psi = 300^\circ$ **for the** $\alpha = -5^\circ$**,** $\theta_{75} = 10^\circ$ **condition**

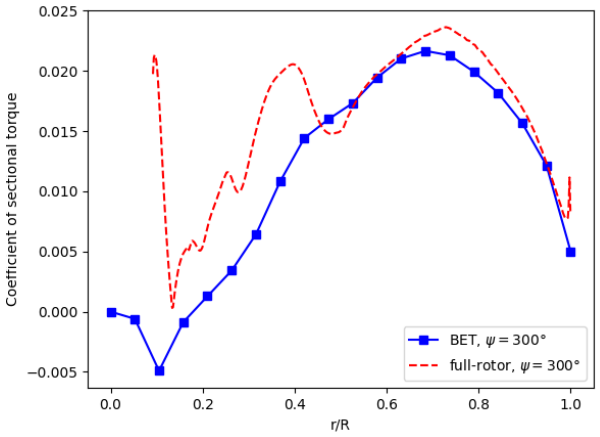

Figure 18. Sectional C_q on blade 1 at $\psi = 300°$ for the $\alpha = -5°$, $\theta_{75} = 10°$ condition

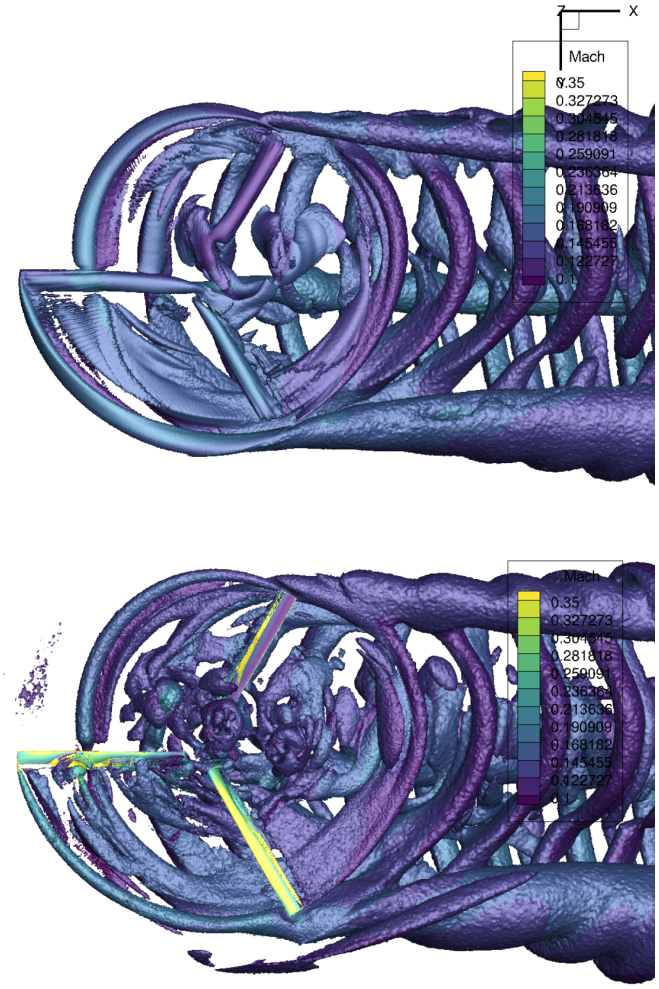

Figure 19. Q-criterion isosurface comparison of the Flow360-BET-Line (top) and Flow360-Full-Rotor simulation (bottom), $\psi = 180°$, $\alpha = -5°$, $\theta_{75} = 10°$

CONCLUSIONS

1. Both the BET-Disk and BET-Line methods show good agreement in terms of C_T and C_Q with both experimental end other high-fidelity CFD results.

2. Accuracy of the sectional loading coefficients for BET-CFD compared to full high-fidelity CFD may show a larger discrepancy, especially near the tip where the flow is highly three-dimensional.

3. Additional work is needed to assess and reduce the sensitivity of the results to the blade line chord, c_{bl}, and the disk thickness, t.

4. Investigation into compressibility effects should be performed in order to assess the sensitivity of the current BET solutions to the effect of compressibility-corrected airfoil polars.

5. The runtime for the BET Disk method is approximately two orders of magnitude lower than a full DDES run, while the runtime for BET-Line is approximately one order of magnitude less than high-fidelity.The BET-RANS method offers good accuracy at a significantly reduced cost.

Author contact: John Moore john@flexcompute.com, Feilin Jia feilin@flexcompute.com, Qiqi Wang qiqi@mit.edu

REFERENCES

1. Anon, "Advancement of Proprotor Technology Task 2 - Wind-Tunnel Test Results," *Nasa Cr 114363*, 1971.

2. F. Felker, L. E. Young, and D. Signor, "Performance and Loads Data from a Hover Test of a Full-Scale Advanced Technology XV-15 Rotor," *Nasa Technical Memorandum 86-854*, no. January 1986, p. 359, 1986.

3. J. S. Light, "Results from an XV-15 rotor test in the national full-scale aerodynamics complex," *Annual Forum Proceedings - American Helicopter Society*, vol. 1, no. May, pp. 231–239, 1997.

4. M. D. Betzina, "Rotor Performance of an Isolated Full-Scale XV-15 Tiltrotor in Helicopter Mode," *American Helicopter Society Aerodynamics, Acoustics, and Test and Evaluation Technical Specialists Meeting*, pp. 1–12, 2002.

5. W. Johnson, *Helicopter Theory*. Dover Publications, 1980.

6. U. K. Kaul and J. Ahmad, "Skin friction predictions over a hovering tilt-rotor blade using OVERFLOW2," *29th AIAA Applied Aerodynamics Conference 2011*, no. June, 2011.

7. S. Yoon, T. H. Pulliam, and N. M. Chaderjian, "Simulations of XV-15 rotor flows in hover using overflow," *American Helicopter Society International - 5th Decennial AHS Aeromechanics Specialists' Conference 2014: Current Challenges and Future Directions in Rotorcraft Aeromechanics*, pp. 365–375, 2014.

8. S. Gates, "Aerodynamic analysis of tiltrotors in hovering and propeller modes using advanced navier-stokes computations," *39th European Rotorcraft Forum 2013, ERF 2013*, pp. 106–109, 2013.

9. A. Jimenez-Garcia, G. Barakos, and S. Gates, "Tiltrotor CFD Part I - validation," *The Aeronautical Journal*, vol. 121, pp. 577–610, 5 2017.

10. M. Field, "A conservative , scalable , space-time blade element rotor model for multirotor vehicles," 2018.

11. K. Uwatoko, M. Kanazaki, H. Nagai, K. Fujita, and A. Oyama, "Blade element theory coupled with cfd applied to optimal design of rotor for mars exploration helicopter," 01 2020.

12. J. Halwick, "Implementation of Blade Element Theory in CFD Analysis of Edgewise Ducted Fan Vehicles," Master's thesis, Pennsylvania State University, 2012.

13. J. Mentey, "Time Dependent Actuator Model for a Helicopter Rotor in Hover," Master's thesis, Pennsylvania State University, 2012.

14. M. Drela, "Xfoil: An analysis and design system for low reynolds number airfoils," vol. 54, 06 1989.